ACS APPLIED MATERIALS & INTERFACES

Research Article

www.acsami.org

Highly Fluorescent Graphene Oxide-Poly(vinyl alcohol) Hybrid: An Effective Material for Specific Au^{3+} Ion Sensors

Aniruddha Kundu, Rama K. Layek, Atanu Kuila, and Arun K. Nandi*

Polymer Science Unit, Indian Association for the Cultivation of Science, Jadavpur, Kolkata-700 032, India

Supporting Information

ABSTRACT: We have developed a new highly fluorescent graphene oxide (GO)/poly(vinyl alcohol) (PVA) hybrid (GO-PVA) in an acidic medium (pH 4). Fourier transform infrared (FTIR) spectra indicate the formation of hydrogen bonds between the hydroxy group of PVA and the hydroxy groups of GO. The hybrid is highly fluorescent, because of passivation by hydrogen bonding, as evident from Raman spectra. The quantum yields of GO-PVA hybrids are higher than that of GO. The fluorescent microscopic images of the hybrids exhibit a fibrillar morphology, and all of them emit highly intense green light. Field-emission scanning electron microscopy (FESEM) micrographs also show a fibrillar morphology, which is produced due to the supramolecular organization of GO-PVA complex. The highly fluorescent GO-PVA1 hybrid has been used as a fascinating tool for selective sensing of Au^{3+} ions in aqueous media with a detectable limit of ~275 ppb. The sensitivity of the Au^{3+} ion (300 μM) in the presence of 600 μM concentrations of each ion (Cu^{2+}, Ag^{+}, Mg^{2+}, Ca^{2+}, Zn^{2+}, K^{+}, Pb^{2+}, Co^{2+}, Ni^{2+}, Pd^{2+}, Fe^{2+}, Fe^{3+}, and Cr^{3+}), taken together, is unique, exhibiting a quenching efficiency of 76%. The quenching efficiency in the presence of a biologically analogous mixture (D-glucose, D-lysine, BSA, Na^{+}, K^{+}, Ca^{2+}, Mg^{2+}, Zn^{2+}) (600 μM each) is 73%, which suggests that the GO-PVA1 hybrid is an efficient sensor of Au^{3+} ions. The average lifetime of GO at pH 4 increases in the GO-PVA1 hybrid, indicating the formation of a more stable excited state but the increase in lifetime value after addition of Au^{3+} salt solution to the hybrid solution indicates dynamic quenching. The selectivity of sensing of Au^{3+} is attributed to its reduction potential being higher than that of other metal ions and XPS data of GO-PVA1 hybrid with 300 μM Au^{3+} substantiate the reduction of Au^{3+} to Au^{0}, because of the transfer of excitons from the hybrid facilitating the selective photoluminescence (PL) quenching.

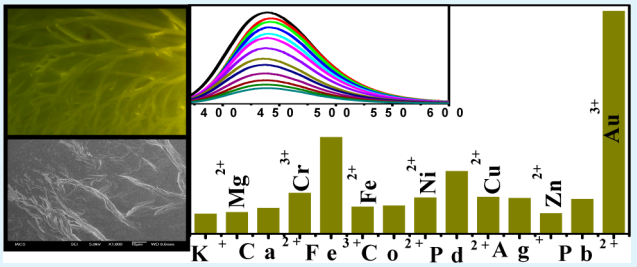

KEYWORDS: *graphene oxide, fluorescence, poly(vinyl alcohol), quenching efficiency, sensor, Raman spectra*

INTRODUCTION

Among the various types of nanomaterials, recently, graphene oxide (GO) has attracted great attention, because of its unique electronic properties arising from the presence of both sp^2 and sp^3 carbons, ensuing promising applications in advanced technologies.[1−13] It consists of a two-dimensional (2D) sheet of covalently decorated C atoms bearing various oxygen functional groups (e.g., hydroxyl, epoxy, and carboxyl) either on the basal plane or at the edges. One of the interesting properties of GO is its propensity to exfoliate spontaneously in aqueous medium into individual sheets to form a stable colloidal suspension.[1,3] However, pure graphene has intrinsic zero band gap, due to the continuous sp^2 hybridized structure, but its hydrophobic properties limit its applications in optoelectronic devices and chemo/biosensing. On the other hand, GO has unique properties such as good dispersity in water and a substantial band gap for the presence of a large amount (~50%) of sp^3 hybridized carbon,[14−16] making it a unique material from graphene and reduced graphene oxide. Its 2D nanostructure and chemical functionality make it highly attractive in nanocomposites,[17] catalysis,[18] drug delivery, and cell imaging,[19,20] as well as in chemo/biosensing.[21]

Recently, the electrogenerated chemiluminescence and photoluminescence (PL) property originating from the chemically prepared GO offer new exciting opportunities in bionanotechnology, such as chemo/biosensing and cell imaging.[19−22] GO gives visible−near infrared (Vis-NIR) fluorescence, which was presumably assigned to the radiative recombination of electron−hole pairs localized within the small sp^2 carbon domains embedded in the sp^3 matrix.[19,23,24] The poor emissive property of GO is due to the hydroxyl, carboxylic, and epoxy groups, which usually induce the nonradiative recombination by the transfer of their electrons to the holes present in sp^2 clusters producing nonradiative localized electron−hole (e-h) pairs.[23,24] Recently, Mei et al.[25] reported water-soluble blue fluorescent GO by amide formation with −COOH groups and epoxide ring opening by alkyl amines destroying the nonradiative electron hole (e-h) recombination centers of GO. Thus, the overall PL property in GO may reflect effects from various sizes of luminescent

Received: July 26, 2012
Accepted: September 26, 2012
Published: September 26, 2012

   dx.doi.org/10.1021/am301467z | ACS Appl. Mater. Interfaces 2012, 4, 5576−5582

carbon domains, and their radiative recombination as well. Very recently, Ajayan et al.[26] and Kochmann et al.[27] have reported on the PL properties of GO and its pH dependency. The former group have proposed that the PL properties of GO arise from the quasi-molecular fluorophores, similar to the polycyclic aromatic compounds formed by the electronic coupling of O atoms of carboxylic acid groups with the nearby C atom of graphene and also observed a strongly pH-dependent fluorescence of GO. They have suggested that the PL properties of GO above pH 8 are due to the electronically excited carboxylate ion of GO. In contrast, the latter group has explained the pH-dependent PL properties of GO, depending on the protonation and deprotonation of −COOH and −OH groups of GO. In our previous article,[28] we have also reported an efficient photoluminescent GO and proposed that the pH response of the photoluminescence of GO is related to the passivation of nonradiative defects embedded in the graphene network. Also, a highly fluorescent GO hybrid has been produced using a biocompatible and nontoxic polymer methyl cellulose,[29,30] and this fluorescent hybrid is used as an efficient nitroaromatic sensor with a detectable limit of 2 ppm for picric acid.[28] Herein, we report an efficient fluorescent GO hybrid in acidic medium prepared by a facile way using a biocompatible, biodegradable, and nontoxic polymer, namely, poly(vinyl alcohol) (PVA)[31−33] and the hybrid is named as GO-PVA. PVA is a hydrophilic polymer with pendent hydroxyl (−OH) groups, which can interact with the −OH, epoxy, or carboxyl groups (−COOH) present on the GO under sonication to form a stable complex, preventing restacking of GO sheets, causing an enhancement of PL intensity.

Currently, much attention has been paid to the development of GO-based sensors for DNA,[34−36] protein,[37] ATP,[38] glucose,[39,40] and metal ions.[41] Among the heavy-metal ions, Au^{3+} is known to be potentially toxic to humans, since soluble gold salts such as gold chloride are recognized to cause damage to the liver, kidneys, and the peripheral nervous system.[42] The Au^{3+} salt solution is over 90% toxic at a concentration of 200 μM.[43] $HAuCl_4$ (10−15 μmol) cause agglutination and hemolysis of erythrocytes suspended in 1 mL of saline.[44,45] Also, some Au ions, especially Au^{3+}, are reported to cause cell toxicity in living organisms, since they can strongly bind to certain enzymes.[46,47] Three Au atoms bind to a single deoxynucleotide; the binding is rapid with d-AMP (d-adenosine monophosphate) and d-GMP (d-guanosine monophosphate) and slow with pyrimidines. Thus, the toxicity of soluble Au^{3+} salts could be attributed to the binding with DNA and also with some enzymes. There are recent reports on the detection of Au^{3+} using fluorescent probe, and mostly all of them involve organic media for the design of the probe.[48−51] However, to detect the Au^{3+} contamination in biological system, the sensing of the Au^{3+} in an aqueous medium is important. Among the other metal ions (e.g., Na^+, K^+, Zn^{2+}, Fe^{2+}, Mg^{2+}, Co^{2+}, Cu^{2+}, Pb^{2+}, Cr^{3+}, Ni^{2+}, Pd^{2+}, Fe^{3+}, etc.), the Au^{3+} is very special for its much higher standard reduction potential (+1.51 V), which may facilitate its specific detection than the others present in the system. Here, we have used the highly fluorescent GO-PVA hybrid in a simple way to develop a specific and efficient fluorescence sensor for Au^{3+} ion in an aqueous medium, based on the PL properties of the hybrid.

EXPERIMENTAL SECTION

Materials. Graphite (Aldrich, USA), and sodium nitrate and potassium permanganate (Merck, Mumbai), were used as-received. PVA (Fluka, $M_w \approx 205\,000$), D-lysine, bovine serum albumin (BSA) (Sigma−Aldrich), and D-glucose (Merck), also were used as-received. $HAuCl_4 \cdot 3H_2O$ (Sigma−Aldrich), $AgNO_3$, NaCl, KCl, $CoCl_2 \cdot 6H_2O$, $MgSO_4 \cdot 7H_2O$, $Cu(CH_3COO)_2 \cdot H_2O$, $Zn(CH_3COO)_2 \cdot 2H_2O$, $Pb(NO_3)_2$, $CaSO_4 \cdot 2H_2O$, anhydrous $FeCl_3$, $FeSO_4 \cdot 7H_2O$, $NiCl_2 \cdot 6H_2O$, $PdCl_2 \cdot 2H_2O$, $[Cr(H_2O)_6](NO_3)_3 \cdot 3H_2O$ (Merck, Mumbai) were used as-received during detection of their respective metal ions.

Preparation of GO-PVA Hybrids. At first, GO was prepared from graphite powder, according to the Hummers and Offeman method, using $NaNO_3$, $KMnO_4$, and H_2SO_4.[52] The produced GO was then dispersed in acidic medium of pH 4, by sonication to make a constant composition (0.005% (w/v)). In the above GO solution, 35, 70, and 140 mg of PVA was added to prepare the GO-PVA hybrids with PVA concentrations of 0.5%, 1.0%, and 2.0% (w/v), respectively, and sonicated for 2 h, using an ultrasonic bath (60 W, frequency of 28 kHz, Model AVIOC, Eyela) to achieve a molecular level dispersion of GO in PVA matrix and the hybrids were designated as GO-PVA0.5, GO-PVA1, and GO-PVA2, respectively. The composition of as-prepared GO-PVA hybrid has been presented in Table 1.

Table 1. Compositions of GO-PVA Hybrid Solution (7 mL) at pH 4

system	GO (%, w/v)	PVA (mg)	PVA (%, w/v)
GO-PVA0.5	0.005	35	0.5
GO-PVA1	0.005	70	1
GO-PVA2	0.005	140	2

Characterization. *Microscopy.* Field-emission scanning electron microscopy (FESEM) was conducted by casting a drop of solution on a silicon wafer and was dried in air and finally in vacuum for three days at 30 °C. The morphology was studied using a FESEM instrument (JEOL, Model GSM-5800). The GO dispersion was characterized by transmission electron microscopy (TEM) (JEOL, Model 2010EX) fitted with a CCD camera at an acceleration voltage of 200 kV. A TEM sample was prepared by spreading a small drop of diluted GO solution on a carbon-coated copper grid and allowing it to dry in air and finally under vacuum at 30 °C for ∼3 days.

The fluorescence microscopy of GO and that of GO-PVA hybrids at pH 4 was made by casting a drop of the solutions on microscopic glass slides and evaporating it in air at 30 °C for three days. The glass slides were then observed through a fluorescence microscope (Olympus, Model BX61) by exciting the sample with a UV radiation of 320 nm using a FITC filter.

Spectroscopy. The UV−vis absorption spectra of aqueous solutions of the samples (GO, and GO-PVA0.5, GO-PVA1, and GO-PVA2), prepared as above, were recorded with a UV−vis spectrophotometer (Hewlett−Packard, Model 8453), using a cuvette with a path length of 1 cm. To perform the photoluminescence (PL) study, the above sample solutions were taken in a sealed cuvette and the emission was studied in a Horiba Jobin−Yvon Fluoromax 3 instrument. Each sample in a quartz cell with a path length of 1 cm was excited at 320 nm wavelength and the emission scans were recorded from 370 nm to 600 nm, using a slit width of 5 nm for both excitation and emission, with an increment wavelength of 1 nm and an integration time of 0.1 s.

Fourier transform infrared (FT-IR) spectra of the samples were obtained from thin films cast from the hybrid solutions on a silicon wafer using a Perkin−Elmer FT-IR instrument (Model spectrum100). Raman spectra of the above GO and GO-PVA solutions were recorded at pH 4 and pH 7, using a LabSpec Raman spectroscope (Model JY T6400). The sample solutions were taken in a quartz cell with a path length of 1 cm and were excited at 514 nm with an Ar-ion laser with a scanning duration of 50 s.

Fluorescence lifetimes were measured using a time-correlated single photon counting fluorimeter (Fluorocube, Horiba Jobin−Yvon). The GO and GO-PVA1 (before and after the addition of Au^{3+} ions) solutions were excited with a 340-nm laser with a pulse duration of <200 ps (nano LED of Horiba Jobin−Yvon). All the samples were prepared for room-temperature measurement (30 °C) in double-

distilled water at pH 4. Average fluorescence lifetimes (τ_f) for exponential interactive fitting were calculated from the decay times (τ_i) and the relative amplitudes (a_i), using the following relation:

$$\langle \tau_f \rangle = a_1\tau_1 + a_2\tau_2 + a_3\tau_3 \quad (1)$$

where a_1, a_2, and a_3 are the relative amplitudes and τ_1, τ_2, and τ_3 are the component lifetimes, respectively.

The X-ray photoelectron spectroscopy (XPS) of GO-PVA1 hybrid film in the presence of 300 μM Au^{3+} ion was performed using a focused monochromatized Mg Kα X-ray source (1253.6 eV) in the XPS instrument (Omicron NanoTechnology 0571).

Photoluminescence Quantum Yield Measurements. The PL quantum yields (QY) of GO and different surface-passivated GO-PVA hybrids before and after addition of Au^{3+} were measured using the same procedure. Quinine sulfate in 0.1 M H_2SO_4 (quantum yield = 0.58 at 340 nm) was chosen as a standard for the fluorescence quantum yield measurement. The values were calculated using the standard reference sample that has a fixed and known fluorescence quantum yield value, according to the following equation:

$$QY_{sample} = QY_{std}\left[\left(\frac{I}{A}\right)_{sample} \times \left(\frac{A}{I}\right)_{std}\right]\left(\frac{\eta^2_{sample}}{\eta^2_{std}}\right)$$

where A is absorbance at the excitation wavelength, η the refractive index, and I the integrated emission intensity calculated from the area under the emission peak on the same wavelength scale.

RESULTS AND DISCUSSION

In Figure 1a, the UV–vis absorption spectra of pure GO and GO-PVA solutions of different concentrations are shown. Pure GO displays two characteristic absorption peaks at 244 and 302 nm (inset) originating from the $\pi-\pi^*$ and $n-\pi^*$ transitions, respectively.The spectrum changes upon the addition of PVA, and both absorption peaks are blue-shifted.The 244-nm peak has shifted to 210, 208, and 204 nm for GO-PVA0.5, GO-PVA1, and GO-PVA2 samples, respectively, while the 302 nm peak has shifted to 258 nm in every case. The above blue shifts may be attributed to the decrease of planarity of GO due to hydrogen bonding with the high-molecular-weight PVA chain,[8,9] resulting in a lesser-conjugated system.

In Figure 1b, PL spectra of the GO solution and that of the GO-PVA hybrids of different compositions are presented at pH 4, keeping the concentration of GO in the hybrid constant (0.005% (w/v)). It is obvious from the spectra that the PL intensity increases dramatically as the PVA concentration in the hybrid increases. The fluorescence enhancement by complexation with PVA may be attributed to the passivation of the GO surface, instead of PVA themselves, because they contain no visible or near-UV fluorophores. The strong interaction between PVA and GO has been confirmed in previous reports,[8,9] and hydrogen bonding is considered to be the dominant force. In Figure S1 in the Supporting Information, the FTIR spectra of the components and GO-PVA hybrids are presented to investigate the interaction between the PVA matrix and the GO sheets. The exfoliated GO exhibits three characteristic peaks at 3424, 1710, and 1060 cm^{-1}, indicating the stretching vibrations of hydroxyl, carbonyl, and epoxy groups, respectively. The –OH stretching peaks (3424 cm^{-1}) of GO are shifted to a lower energy vibration at 3353 and 3265 cm^{-1} in GO-PVA0.5 and the GO-PVA1 hybrid, which suggested hydrogen bonding interactions between PVA and GO sheets. A schematic model of supramolecular interaction is presented in Scheme 1.

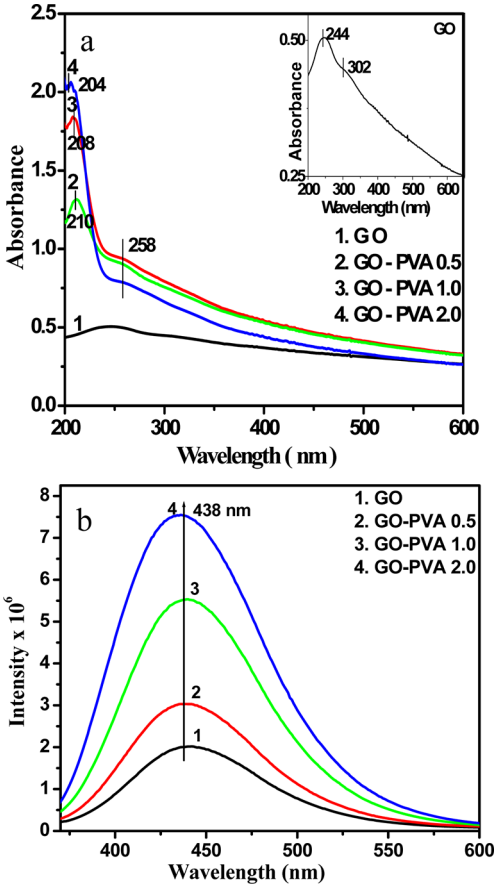

Figure 1. (a) UV–vis spectra and (b) PL spectra of GO and GO-PVA hybrids of different composition at pH 4.

Scheme 1. Schematic Illustration of Supramolecular Interactions between GO and PVA

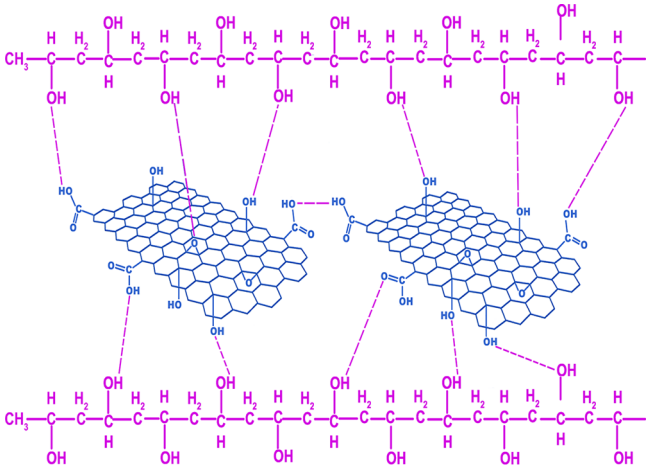

In Table 2, the fluorescence quantum yield of GO and different surface-passivated GO-PVA hybrids are presented. It is evident from the table that the quantum yields (%) in GO-PVA hybrids are higher than that of GO, which suggests that the decay of excitons by nonradiative electron–hole recombination decreases because of the different degree of surface passivation of GO. It increases as the PVA concentration increases, because of different degrees of hydrogen bonding yielding higher quantum yields. The hydrogen bonds produced from various

dx.doi.org/10.1021/am301467z | ACS Appl. Mater. Interfaces 2012, 4, 5576–5582

Table 2. Quantum Yields of Different Hybrid Systems at pH 4

system	quantum yield, Φ (%)
GO	1.41
GO-PVA0.5	2.41
GO-PVA1	2.88
GO-PVA2	3.03
GO-PVA1-Au^{3+} (100 μM)	1.42
GO-PVA1-Au^{3+} (200 μM)	1.11
GO-PVA1-Au^{3+} (300 μM)	0.87

functional groups of GO with the hydroxyl-rich PVA chains cause passivation of the graphene network. The decrease of planarity of GO due to hydrogen bonding results in a lesser-conjugated system decreasing the nonradiative recombination of the electron−hole pair and, hence, improves the emission efficiency of the sp^2 domains on GO nanosheets. Another reason may be the strong hydrogen-bonding interaction, which inhibits nonradiative electron−hole recombination by reducing the electron-donating capability of epoxy, hydroxyl, and carboxylic acid groups of GO to the holes of graphene rings at the excited state, accounting for the enhancement of the PL intensity. The hydrogen-bonded PVA prevents the quenching of excitons with the solvent molecules (water), which also contributes to the increase in PL intensity. Thus, the passivation of GO by PVA could be a combined effect of all three of the above factors.

The Raman spectrum of GO (Figure 2) at pH 4 shows the D band (doublet) at 1388 and 1469 cm^{-1} and G band at 1613 cm^{-1}. In the GO-PVA hybrids, both the D band and the G band shift to lower wavenumber and the intensity ratio of D band to G band has increased (1.01, 1.14, 1.28 for GO, GO-PVA0.5, GO-PVA1, respectively) with increasing PVA concentration at pH 4. Both the D and G bands arise due to skeletal vibrations of GO at the sp^3- and sp^2-rich domains, respectively. After complexation with PVA, the π-electrons of graphene rings become somewhat delocalized, making vibration of the skeleton and shifting the above bands to lower energy easier. Also, the increase of intensity ratio of the D band and G band indicates increased disorderness (i.e., sp^3 character), because of hydrogen bonding with PVA (see Table 3). To understand the origin of the doublet, it is necessary to compare the D band of GO, GO-PVA0.5, GO-PVA1 at pH 4 with those at pH 7 (see Figure S2 in the Supporting Information), where it exhibits a singlet in the range of 1352−1355 cm^{-1}. This lower-energy skeleton vibration at pH 7 is due to the increased delocalization of ring electrons, because of resonance with the carboxylate ion. The D/G intensity ratio of GO-PVA hybrids at pH 7 remains almost the same as that of GO, because of the ionization of the carboxylic acid group. However, at pH 4, the un-ionized carboxylic acid group does not take part in resonance delocalization of the ring electron to the same extent, causing a shift to higher energy (1388 and 1469 cm^{-1}). The doublet nature of the D band of GO at this pH may be attributed to the two different types of sp^3 skeletons present at the GO: presumably one resides in the bulk and the other resides at the side being severely passivated at pH 4.

Table 3. D/G Ratio of GO and GO-PVA 0.5, GO-PVA 1 at Indicated pH Values

	D/G ratio	
system	pH 4	pH 7
GO	1.01	0.94
GO-PVA0.5	1.14	0.91
GO-PVA1	1.28	0.91

The fluorescent micrographs of GO and GO-PVA hybrids at pH 4 are presented in Figure 3a−d. The fluorescent images of the hybrid clearly indicates that GO-PVA hybrids have fibrillar morphology and the fibrils are emitting fluorescent green light.

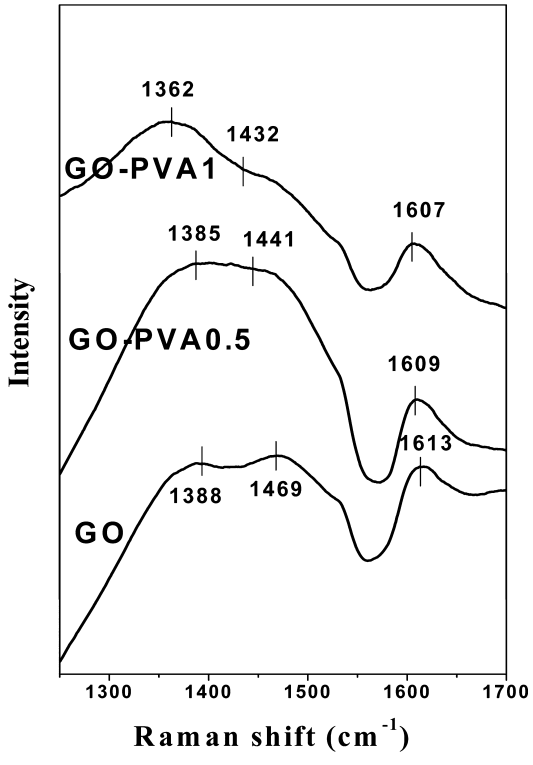

Figure 2. Raman spectra of GO, GO-PVA0.5, and GO-PVA1.

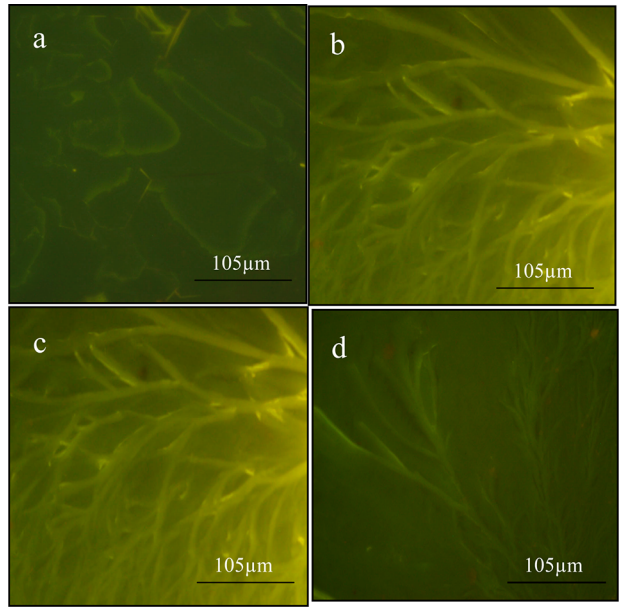

Figure 3. Fluorescence micrographs of (a) GO, (b) GO-PVA0.5, (c) GO-PVA1, and (d) GO-PVA2 at pH 4.

dx.doi.org/10.1021/am301467z | ACS Appl. Mater. Interfaces 2012, 4, 5576−5582

The high-resolution transmission electron microscopy (HRTEM) image indicates the exfoliated nature of the GO sheet (see Figure S3 in the Supporting Information). FESEM micrographs of the GO-PVA0.5 and GO-PVA1 hybrids (Figure S3 in the Supporting Information) also show a fibrillar morphology. Hence, the formation of a fibrillar morphology for all of the hybrids can be attributed to the hydrogen-bonding interaction between GO and PVA, followed by the supramolecular organization of the GO-PVA complex (recall Scheme 1) producing the fibrils.

Now, to study the effect of different metal ions on the optical properties of the hybrid, we have chosen the GO-PVA1 hybrid solution, which has been titrated with the salts of Au^{3+}, Cu^{2+}, Ag^{+}, Mg^{2+}, Ca^{2+}, Zn^{2+}, K^{+}, Pb^{2+}, Co^{2+}, Ni^{2+}, Pd^{2+}, Fe^{2+}, Fe^{3+}, and Cr^{3+}, using fluorescence spectroscopy (see Figure 4a and Figures S4–S16 in the Supporting Information). Among these ions, Au^{3+} chloride causes fluorescence quenching of the GO-PVA1 hybrid to a very large extent (~83%), whereas all of the other metal salts have a negligible effect or virtually no effect on the fluorescence of the hybrid, even for higher concentrations (600 μM) of metal ions (Figure 4b). Fe^{3+} usually acts as a good fluorescence quencher; in 300 μM Fe^{3+}, the quenching efficiency is 23% and, in 600 μM, it is 35% (see Figure S15 in the Supporting Information). Both are much less than that of the 300 μM Au^{3+} solution (83%), facilitating the specific sensing of Au^{3+}. The calibration curve for Au^{3+} detection is shown in Figure 5, where I_0/I (I_0 is the PL intensity of the GO-PVA1 hybrid and I is that upon the gradual addition of Au^{3+}) is plotted with Au^{3+} concentration. The concentration of any Au^{3+} solution can be estimated easily from the measurement of the above intensity ratio and comparing the data with the calibration curve.

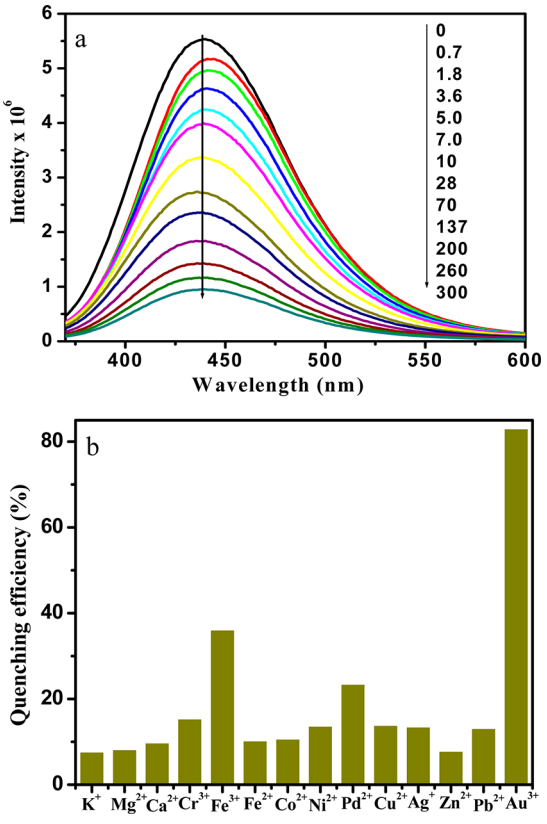

Figure 4. (a) Fluorescence titration of GO-PVA1 upon gradual addition of Au^{3+} solution (μM). (b) Bar diagram showing quenching efficiencies for addition of different metal ions (600 μM) and an Au^{3+} ion concentration of 300 μM.

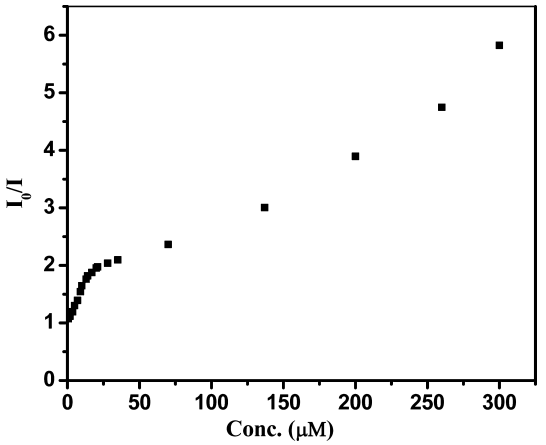

Figure 5. Calibration curve for the detection of Au^{3+}, where I_0 is the intensity of the GO-PVA1 hybrid and I is the intensity upon the gradual addition of Au^{3+}.

The effect of different metal ions at the 300 μM concentration on the fluorescence quenching of GO-PVA1 hybrid has also been shown in Figure S17 in the Supporting Information and the quenching efficiency is certainly highest for Au^{3+} ions. The sensitivity of the Au^{3+} ion in the presence of 600 μM concentrations of each ion, taken together, has been presented in Figure S18 in the Supporting Information and its quenching efficiency is 76%. Therefore, it is clear from the figure that GO-PVA1 acts as an efficient specific sensor of Au^{3+} ions, even in the mixture of other ions with double the Au^{3+} concentration. Again, the sensitivity of Au^{3+} in the presence of a biologically analogous mixture (D-glucose, D-lysine, BSA, Na^{+}, K^{+}, Ca^{2+}, Mg^{2+}, Zn^{2+}) (600 μM each) has been studied and is presented in Figure S19 in the Supporting Information. It is evident from the figure that an initial 10% decrease in PL intensity occurs upon the addition of the biologically analogous mixture to the GO-PVA1 system. Upon the addition of Au^{3+} ions, the PL intensity of the system gradually decreases and, for the 300 μM Au^{3+} solution, the PL quenching is 73% from that of pure GO-PVA1 system and 70% from that of the biological mixture. Therefore, this result supports that the GO-PVA1 system is really useful as an efficient Au^{3+} sensor in biological systems. The GO-PVA1 system does not exhibit any detectable change in PL intensity in industrial wastewater (Bantala, Kolkata), suggesting the absence of Au^{3+} ions in this wastewater (see Figure S20 in the Supporting Information); however, upon the addition of 300 μM Au^{3+} to it, a 42% decrease in PL intensity occurs (see Figure S21 in the Supporting Information). Upon the wastewater addition of 300 μM Au^{3+}, the solution becomes turbid (pH 7.6), causing a partial quenching (less than the 83% that occurred in a transparent Au^{3+} solution at pH 4). However, upon the addition of the same amounts of Fe^{3+} to the hybrid solution, no PL quenching occurs at this high pH of wastewater; instead, precipitation of Fe^{3+} is observed. Hence, the Au^{3+} ion is detectable, if present, in industrial wastewater, compared to other metal ions.

Such a significant and instant quenching of the GO-PVA1 hybrid by Au^{3+} is interesting and may be attributed to an easier transfer of excitons from GO-PVA1 to Au^{3+} ions.[53] The higher reduction potential of the Au^{3+}/Au system, compared to the

Table 4. Lifetime Values of GO and GO-PVA1 before and after the Addition of Au^{3+} Salt Solution[a]

system	τ_1 (ns)	a_1	τ_2 (ns)	a_2	τ_3 (ns)	a_3	τ_4 (ns)	a_4	$\langle\tau\rangle$ (ns)
GO	0.05	15.02	1.15	4.94	3.78	70.13	7.17	9.91	3.42
GO-PVA1	3.15	42.15	5.8	39.98	0.7	17.87			3.77
GO-PVA1-Au^{3+} (0.7 μM)	2.12	17.09	5	72.62	0.06	10.29			4.0
GO-PVA1-Au^{3+} (300 μM)	2.3	23.17	5.26	68.38	0.08	8.45			4.13

[a]Parameters a_1, a_2, a_3, and a_4 indicate relative amplitudes.

other metal ions, is the probable cause of selective sensing of Au^{3+} by the hybrid, since the exciton of GO-PVA1 gets easily transferred to the Au^{3+} ions, causing significant PL quenching. From Figure 4a, it is apparent that the detectable response of Au^{3+} ions for the GO-PVA1 system is found to be 275 ppb (0.7 μM).

To obtain an insight into the excitonic dynamics, we have measured the fluorescence lifetime values of GO and GO-PVA1 before and after the addition of Au^{3+} salt solution at pH 4 from the decay curves (see Figure S22 in the Supporting Information), and the average lifetime values, together with the component decay times, are presented in Table 4. It is obvious from the table that the average lifetime of GO at pH 4 increases in the GO-PVA1 hybrid, indicating the formation of a more-stable excited state, because of the supramolecular interaction of GO with PVA. However, the increase in lifetime value after the addition of Au^{3+} salt solution to the hybrid solution indicates dynamic quenching, as a result of excitonic transfer from the electronically rich GO-PVA1 hybrid to the electronically deficient Au^{3+}, causing a decrease in the mean decay time of the entire excited-state population.[54]

To investigate the end product of the exciton transfer from the electronically rich GO-PVA1 hybrid to the Au^{3+} ion, we have performed an XPS study of the Au^{3+} ion (300 μM) treated GO-PVA1 hybrid film. From the survey scan XPS spectra (Figure S23 in the Supporting Information), it is obvious that the peaks at ~285.9 eV and ~533.4 eV correspond to the C 1s and O 1s core levels, respectively, and, from Figure 6, it is

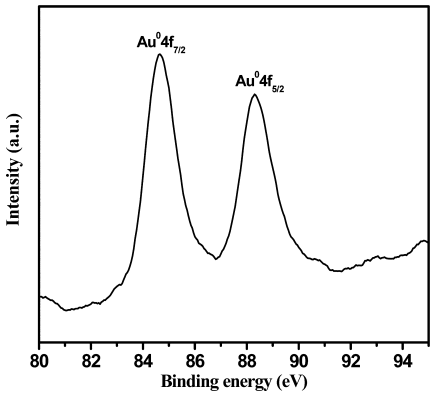

Figure 6. XPS spectrum of Au^0 4f peak of the GO-PVA1 hybrid film in the presence of Au^{3+} ion (300 μM).

evident that Au^{3+} has been reduced to gold metal (Au^0) by the excitons of the GO-PVA hybrid, as indicated from the Au $4f_{7/2}$ and Au $4f_{5/2}$ doublet peaks located at 84.6 and 88.3 eV, respectively.[53,55] This has been ascribed to the higher reduction potential of Au^{3+}, and this reduction process is the cause of the PL quenching of GO-PVA1 hybrid upon the gradual addition of Au^{3+} into it.

CONCLUSION

This work presents a simple strategy to prepare a highly fluorescent graphene oxide (GO) hybrid, in which the polymer PVA acts both as a spacer, preventing GO sheets from restacking in the assembly, and also causing passivation to the electron−hole recombination process, yielding a higher PL intensity. Au^{3+} acts as an effective quenching agent, allowing the GO-PVA system to act as a specific sensor of the toxic Au^{3+} ions in aqueous medium. To the best of our knowledge, it is the first time that anyone has reported the sensing of Au^{3+} ions in an aqueous medium, extending its probable use in biological systems.

ASSOCIATED CONTENT

Supporting Information

FTIR spectra of GO, PVA, GO-PVA0.5, and GO-PVA1 at pH 4; Raman spectra of GO, GO-PVA0.5, and GO-PVA1 at pH 7; HRTEM image of GO and FESEM images of PVA, GO-PVA0.5, and GO-PVA1 at pH 4; PL spectra of GO-PVA1 hybrid in the presence of Cu^{2+}, Ag^{+}, Mg^{2+}, Ca^{2+}, Zn^{2+}, K^{+}, Pb^{2+}, Co^{2+}, Ni^{2+}, Pd^{2+}, Fe^{2+}, Fe^{3+}, and Cr^{3+}, and the sensitivity of Au^{3+} in the presence of the other metal ions, biologically analogous mixture, and wastewater; bar diagram showing quenching efficiencies of different metal ions; fluorescence lifetime plots of GO and GO-PVA1 before and after the addition of Au^{3+} salt solution at pH 4; survey scan XPS spectra of GO-PVA1 hybrid film in the presence of Au^{3+} ion, etc. This information is available free of charge via the Internet at http://pubs.acs.org/.

AUTHOR INFORMATION

Corresponding Author

*Fax: (+91) 33 2473 2805. E-mail: psuakn@iacs.res.in.

Notes

The authors declare no competing financial interest.

ACKNOWLEDGMENTS

We gratefully acknowledge DST (Grant No. SR/S1/PC/26/2009) New Delhi and DST Unit of Nanoscience at IACS for financial support. A. Kundu, R.K.L., and A. Kuila gratefully acknowledge CSIR, New Delhi, for granting their fellowships.

REFERENCES

(1) Compton, O. C.; Nguyen, S. T. *Small* **2010**, *6*, 711−723.
(2) Allen, M. J.; Tung, V. C.; Kaner, R. B. *Chem. Rev. (Washington, DC, U.S.)* **2009**, *110*, 132−145.
(3) Dreyer, D. R.; Park, S.; Bielawski, C. W.; Ruoff, R. S. *Chem. Soc. Rev.* **2010**, *39*, 228−240.
(4) Zhang, C.; Ren, L. L.; Wang, X. Y.; Liu, T. X. *J. Phys. Chem. C* **2010**, *114*, 11435−11440.
(5) Paci, J. T.; Belytschko, T.; Schatz, G. C. *J. Phys. Chem. C* **2007**, *111*, 18099−18111.
(6) Navarro, C. G.; Burghard, M.; Kern, K. *Nano Lett.* **2008**, *8*, 2045−2049.

(7) Zhao, X.; Zhang, Q. H.; Chen, D. J. *Macromolecules* **2010**, *43*, 2357−2363.
(8) Liang, J. J.; Huang, Y.; Zhang, L.; Wang, Y.; Ma, Y. F.; Guo, T. Y.; Chen, Y. S. *Adv. Funct. Mater.* **2009**, *19*, 2297−2302.
(9) Xu, Y. X.; Hong, W. J.; Bai, H.; Li, C.; Shi, G. Q. *Carbon* **2009**, *47*, 3538−3543.
(10) Yang, X. M.; Li, L.; Shang, S. M.; Tao, X. M. *Polymer* **2010**, *51*, 3431−3435.
(11) Rafiee, M. A.; Rafiee, J.; Wang, Z.; Song, H. H.; Yu, Z. Z.; Koratkar, N. *ACS Nano* **2009**, *3*, 3884−3890.
(12) Rafiee, M. A.; Rafiee, J.; Srivastava, I.; Wang, Z.; Song, H. H.; Yu, Z. Z.; Koratkar, N. *Small* **2010**, *6*, 179−183.
(13) Kuila, T.; Bhadra, S.; Yao, D. H.; Kim, N. H.; Bose, S.; Lee, J. H. *Prog. Polym. Sci.* **2010**, *35*, 1350−1375.
(14) Cai, W.; Piner, R. D.; Stadermann, F. J.; Park, S.; Shaibat, M. A.; Ishii, Y.; Yang, D.; Velamakanni, A.; An, S. J.; Stoller, M.; An, J.; Chen, D.; Ruoff, R. S. *Science* **2008**, *321*, 1815−1817.
(15) Yang, D.; Velamakanni, A.; Bozoklu, G.; Park, S.; Stoller, M.; Piner, R.; Stankovich, S.; Jung, I.; Field, D.; Ventricejr, C.; Ruoff, R. S. *Carbon* **2009**, *47*, 145−152.
(16) Novoselov, K. S.; Geim, A. K.; Morozov, S. V.; Jiang, D.; Zhang, Y.; Dubonos, S. V.; Grigorieva, I. V.; Firsov, A. A. *Science* **2004**, *306*, 666−669.
(17) Dikin, D. A.; Stankovich, S.; Zimney, E. J.; Piner, R. D.; Dommett, G. H. B.; Evmenenko, G.; Nguyen, S. T.; Ruoff, R. S. *Nature (London, U.K.)* **2007**, *448*, 457−460.
(18) Scheuermann, G. M.; Rumi, L.; Steurer, P.; Bannwarth, W.; Mulhaupt, R. *J. Am. Chem. Soc.* **2009**, *131*, 8262−8270.
(19) Sun, X.; Liu, Z.; Welsher, K.; Robinson, J.; Goodwin, A.; Zaric, S.; Dai, H. *Nano Res.* **2008**, *1*, 203−212.
(20) Liu, Z.; Robinson, J. T.; Sun, X.; Dai, H. *J. Am. Chem. Soc.* **2008**, *130*, 10876−10877.
(21) Lu, C. H.; Yang, H. H.; Zhu, C. L.; Chen, X.; Chen, G. N. *Angew. Chem., Int. Ed.* **2009**, *48*, 4785−4787.
(22) Fan, F. R. F.; Park, S.; Zhu, Y.; Ruoff, R. S.; Bard, A. J. *J. Am. Chem. Soc.* **2008**, *131*, 937−939.
(23) Eda, G.; Lin, Y. Y.; Mattevi, C.; Yamaguchi, H.; Chen, H. A.; Chen, I. S.; Chen, C. W.; Chhowalla, M. *Adv. Mater. (Weinheim, Ger.)* **2010**, *22*, 505−509.
(24) Luo, Z. T.; Vora, P. M.; Mele, E. J.; Johnson, A. T. C.; Kikkawa, J. M. *Appl. Phys. Lett.* **2009**, *94*, 111909−111911.
(25) Mei, Q.; Zhang, K.; Guan, G.; Liu, B.; Wang, S.; Zhang, Z. *Chem. Commun. (Cambridge, U. K.)* **2010**, *46*, 7319−7321.
(26) Galande, C.; Mohite, A. D.; Naumov, A. V.; Gao, W.; Ci, L.; Ajayan, A.; Gao, H.; Srivastava, A.; Weisman, R. B.; Ajayan, P. M. *Sci. Rep.* **2011**, *1: 85*, 1−5.
(27) Kochmann, S.; Hirsch, T.; Wolfbeis, O. S. *J. Fluoresc.* **2012**, *22*, 849−855.
(28) Kundu, A.; Layek, R. K.; Nandi, A. K. *J. Mater. Chem.* **2012**, *22*, 8139−8144.
(29) Martin, B. C.; Minner, E. J.; Wiseman, S. L.; Klank, R. L; Gilbert, R. J. *J. Neural Eng.* **2008**, *5*, 221−231.
(30) Miyamoto, T.; Takahasi, S.; Ito, H.; Inagaki, H. *J. Biomed. Mater. Res.* **1989**, *23*, 125−133.
(31) Burczak, K.; Gamian, E.; Kochman, A. *Biomaterials* **1996**, *17*, 2351−2356.
(32) Deb Nath, D. C.; Bandyopadhyay, S.; Boughton, P.; Yu, A.; Blackburn, D.; White, C. *J. Appl. Polym. Sci.* **2010**, *117*, 114−121.
(33) Demerlis, C. C.; Schoneker, D. R. *Food Chem. Toxicol.* **2003**, *41*, 319−326.
(34) He, S.; Song, B.; Li, D.; Zhu, C.; Qi, W.; Wen, Y.; Wang, L.; Song, S.; Fang, H.; Fan, C. *Adv. Funct. Mater.* **2010**, *20*, 453−459.
(35) Lu, C. H.; Li, J.; Liu, J. J.; Yang, H. H.; Chen, X.; Chen, G. N. *Chem.—Eur. J.* **2010**, *16*, 4889−4894.
(36) Dong, H.; Gao, W.; Yan, F.; Ji, H.; Ju, H. *Anal. Chem.* **2010**, *82*, 5511−5517.
(37) Chang, H.; Tang, L.; Wang, Y.; Jiang, J.; Li, J. *Anal. Chem.* **2010**, *82*, 2341−2346.
(38) Wang, Y.; Li, Z.; Hu, D.; Lin, C. T.; Li, J.; Lin, Y. *J. Am. Chem. Soc.* **2010**, *132*, 9274−9276.
(39) Zhang, C.; Yuan, Y.; Zhang, S.; Wang, Y.; Liu, Z. *Angew. Chem., Int. Ed.* **2011**, *50*, 6851−6854.
(40) Song, Y.; Qu, K.; Zhao, C.; Ren, J.; Qu, X. *Adv. Mater. (Weinheim, Ger.)* **2010**, *22*, 2206−2210.
(41) Wen, Y.; Xing, F.; He, S.; Song, S.; Wang, L.; Long, Y.; Li, D.; Fan, C. *Chem. Commun. (Cambridge, U.K.)* **2010**, *46*, 2596−2598.
(42) Block, W. D.; Knapp, E. L. *J. Pharmacol. Exp. Ther.* **1945**, *83*, 275−278.
(43) Connor, E. E.; Mwamuka, J.; Gole, A.; Murphy, C. J.; Wyatt, M. D. *Small* **2005**, *1*, 325−327.
(44) Jandl, J. H.; Simmons, R. L. *Br. J. Hamaetol.* **1957**, *3*, 19−22.
(45) Luckey, T. D.; Venugopal, B.; Hutcheson, D. *Heavy Metal Toxicity, Safety and Hormology*; Academic Press: New York, 1975; p 16.
(46) Lee, M. T.; Ahmed, T.; Friedman, M. E. *J. Enzyme Inhib.* **1989**, *3*, 23−33.
(47) Jones, J. R. E. *J. Exp. Biol.* **1940**, *17*, 408−415.
(48) Yang, Y. K.; Lee, S.; Tae, J. *Org. Lett.* **2009**, *11*, 5610−5613.
(49) Jou, M. J.; Chen, X.; Swamy, K. M. K.; Kim, H. N.; Kim, H. J.; Lee, S.; Yoon, J. *Chem. Commun. (Cambridge, U.K.)* **2009**, 7218−7220.
(50) Dong, M.; Wang, Y. W.; Peng, Y. *Org. Lett.* **2010**, *12*, 5310−5313.
(51) Yuan, L.; Lin, W.; Yang, Y.; Song, J. *Chem. Commun. (Cambridge, U.K.)* **2011**, *47*, 4703−4705.
(52) Hummers, W. S.; Offeman, R. E. *J. Am. Chem. Soc.* **1958**, *80*, 1339−1339.
(53) Benayad, A.; Shin, H. J.; Park, H. K.; Yoon, S. M.; Kim, K. K.; Jin, M. H.; Jeong, H. K.; Lee, J. C.; Choi, J. Y.; Lee, Y. H. *Chem. Phys. Lett.* **2009**, *475*, 91−95.
(54) Lakowicz, J. R. *Principles of Fluorescence Spectroscopy*; 3rd ed.; Springer: New York, 2006; p 97.
(55) Wagner, C. D.; Riggs, W. M.; Davis, L. E.; Moulder, J. F.; Muilenberg, G. E. *Handbook of X-ray Photoelectron Spectroscopy*; Perkin−Elmer Corporation: Eden Prairie, MN, 1978.